Resonance, Auger, and Autoionization Processes Involving He$^+$(2s) and He^{++} near Solid Surfaces

H. D. Hagstrum and G. E. Becker

Bell Laboratories, Murray Hill, New Jersey 07974

(Received 9 Feburary 1973)

Electronic transition processes of a resonance and of an Auger type which can occur at a solid surface have been studied for incident metastably excited He$^+$(2s) and doubly charged He^{++} ions. Atomically clean Ni(100) and Ni(110) surfaces have been used as well as these surfaces with a c(2×2)Se structure adsorbed upon them. It is shown that the principal process of deexcitation of the He$^+$(2s) ion involves resonance tunneling to a doubly excited He^{0**} state of the He atom followed by its autoionization to the ground-state ion He$^+$(1s) with the ejection of a fast electron. Autoionized electrons produced near the surface are 0.7–0.9 eV faster than those produced in free space. The change in the work function from 4.7 eV for Ni(110) to 5.1 eV for Ni(100) reduces the number of peaks of ejected electrons from two to one. These experimental facts are shown to be self-consistent and to arise from energy-level shifts near the solid surface. Several aspects of the kinetics of the two-stage processes in competition with possible single-stage processes are discussed. It is also demonstrated that He^{++} is first resonance neutralized by one electronic charge to the He$^+$(2s) state, which process is then followed, closer to the surface, by those observed for incident He$^+$(2s).

I. INTRODUCTION

The radiationless electronic transitions which can occur between an atom or molecule and a solid as the particle approaches or recedes from the surface constitute an important element of the physics of particle-solid interactions. The electrons ejected by the conversion of potential energy have been a principal monitor of these processes. Investigation of such electron-ejection processes are best made at very low incident energy where the potential energy processes predominate completely over those involving conversion of kinetic energy. Comprehensive reviews have been published by Kaminsky[1] and by Abroyan, Eremeev, and Petrov,[2] while Arifov has reviewed work done at Tashkent and has edited a volume of papers from the same institution.[3,4] A number of important papers have appeared since these reviews involving incident ions[5-8] and incident metastable atoms.[9-16] Also, particle-solid electronic interaction is clearly involved in the phenomenon of surface ionization of an incident neutral or excited atom[9,10,17] in which no electrons are ejected from the system.

In the work done to date with incident ions or excited atoms a great variety of types of particle have been used. These include ground state and excited singly charged ions as well as metastable atoms of the noble gases, simple molecular ions and atomic ions derived from simple molecules, and multiply charged ions. In earlier work by one of the present authors (HDH) both multiply charged ions[17-20] and excited singly charged ions[21,22] were employed. Yield as a function of ion energy and kinetic energy distributions of ejected electrons were measured in many cases, and the possibilities as to specific

processes were discussed, but it cannot be said that any of this work was complete or definitive. One can expect to achieve as complete an understanding as possible only if known surfaces of crystalline solids with known work functions are used and studies are made as a function of the kinetic energy of the incident particle.

One arm of our work with ion-solid electronic interactions has been the development of a viable electron spectroscopy of the occupied electron energy levels at solid surfaces based on the Auger-type process by which slowly moving ions are neutralized at solid surfaces.[23-25] It was in the hope that we could significantly extend the basis of this work that we undertook what became the present study using the metastably excited ion He$^+$(2s). The question at issue was whether this ion would deexcite directly to the ground-state ion He$^+$(1s) at the surface in an Auger process, with all the excitation energy being used to excite an electron provided by the solid. If this process were to occur it could form the basis of an important electron spectroscopy because it is energetic (40.8 eV is available as excitation energy) and because its one-electron-like character relates the observed kinetic energy distribution of ejected electrons directly to the surface local density of the electron states rather than to its self-convolution as in the case of a two-electron Auger ejection process. But, as we shall see, this was not to be, because this and related processes are largely obscured by the two-stage process of resonance neutralization of He$^+$(2s) to doubly excited states He^{0**} of the uncharged atom, followed by autoionization to the ground-state ion He$^+$(1s) with the release of an energetic electron. The observed dependence of the reso-

nance process on the surface work function and the atomic character of the subsequent autoionization has made possible, however, a more detailed study of the energetics of this process than has been possible for any other particle-solid electronic process. We also have carried out in this work studies employing the He^{++} ion. A preliminary report on some of the material in the present paper has been published.[26]

The material presented in this paper and its organization is as follows: First, in Sec. II, we identify and discuss atom-solid electronic transition processes both generally and with respect to the specific results of the present work. This is followed, in Sec. III, by a brief statement concerning experimental apparatus and procedures and, in Sec. IV, by a presentation of the experimental results for the $He^+(2s)$ ion incident on clean Ni(100) and Ni(110) surfaces as well as surfaces derived from these by the adsorption of Se atoms in an ordered $c(2 \times 2)$ array. A discussion of the processes which are responsible for the observed electrons is given in Sec. V. In Sec. VI we discuss the energetics and in Sec. VII the kinetics of the dominant two-stage resonance neutralization and autoionization process occurring for incident $He^+(2s)$ ions. Finally, the He^{++} results are presented and discussed in Sec. VIII.

II. ATOM-SOLID ELECTRONIC TRANSITIONS FOR INCIDENT PARTICLES CARRYING POTENTIAL ENERGY

An important class of atom-solid electronic transitions is characterized by the specification that the particle initially possess potential energy by virtue of being excited or ionized or both. Electronic transition processes involving such particles fall into two classes: The one-electron, resonance processes and the two-electron, Auger-type processes. Examples of the two possible resonance processes and the three possible Auger-type processes are given in Table I.

The notation used in Table I is as follows: The atomic particle is indicated by X with its charge state indicated by the superscripts $0, +, ++$, for neutral atom, singly charged ion, and doubly charged ion, respectively. Excitation of a single electron in the particle is indicated by a single asterisk $*$, double excitation by $**$. An electron initially or finally resident in a band state of the solid is indicated by e_S^- with its energy below the vacuum level given as the negative quantity in parentheses following this symbol. The electron which is excited in the Auger-type processes and which may be ejected from the atom-solid system is indicated as e^- without subscript, followed in parentheses by its kinetic energy above the vacuum level. Atomic excitation energies are indicated by E_e, ionization energies by E_i. Superscripts indicating charge

and excitation states attached to E_e refer to the *final* state of a process involving the excitation of a single electron. Superscripts attached to E_i refer to the *initial* state of an ionization process in which one electron is removed from the atom. A prime (') indicates the effective value of an energy near the solid surface as opposed to its value in free space. The energies α, β, and γ are variable quantities which may assume values appropriate to the energies of the filled states in the solid.

The resonance processes of neutralization and ionization (category A of Table I) are in a sense inverse processes but occur for different relative configurations of the electronic states of atomic particle and solid. Resonance neutralization (RN) occurs when the energy level, written generally as $-E$, of the electron $e_S^-(-E)$ lies in the filled states of the solid below the Fermi level, i.e., when $E > \phi$, ϕ being the work function of the solid. Resonance ionization (RI) occurs when $-E$ places the electron e_S^- in the unfilled states of the solid above the Fermi level, $E < \phi$. Resonance ionization of

---

TABLE I. Atom-solid electronic transition processes.

A. One-electron resonance neutralization (RN $\rightarrow$) and resonance ionization (RI $\leftarrow$)

1. $X^+ + e_S^-(-E_1^0{}') \rightleftarrows X^0$

2. $X^+ + e_S^-(-E_i^{0*}{}') \rightleftarrows X^{0*}$

3. $X^{+*} + e_S^-(-E_i^{0**}{}') \rightleftarrows X^{0**}$

4. $X^{++} + e_S^-(-E_i^+{}') \rightleftarrows X^+$

5. $X^{++} + e_S^-(-E_i^{+*}{}') \rightleftarrows X^{+*}$

B. Two-electron Auger deexcitation (AD)

1. $X^{0*} + e_S^-(-\alpha) \rightarrow X^0 + e^-(E_e^{0*}{}' - \alpha)$

2. $X^{0**} + e_S^-(-\alpha) \rightarrow X^{0*} + e^-(E_e^{0**}{}' - E_e^{0*}{}' - \alpha)$

3. $X^{+*} + e_S^-(-\alpha) \rightarrow X^+ + e^-(E_e^{+*}{}' - \alpha)$

C. Two-electron Auger neutralization (AN)

1. $X^+ + e_S^-(-\alpha) + e_S^-(-\beta) \rightarrow X^0 + e^-(E_i^0{}' - \alpha - \beta)$

2. $X^{++} + e_S^-(-\alpha) + e_S^-(-\beta) \rightarrow X^{0*} + e^-(E_i^0{}' + E_e^{+*}{}' - \alpha - \beta)$

3. $X^{++} + e_S^-(-\alpha) + e_S^-(-\beta) \rightarrow X^0 + e^-(E_i^0{}' + E_e^{+*}{}' - \alpha - \beta)$

D. Two-electron autionization (AI)

$X^{0**} \rightarrow X^+ + e^-(E_e^{0**}{}' - E_i^0{}')$

E. Three-electron ion neutralization

$X^{++} + e_S^-(-\alpha) + e_S^-(-\beta) + e_S^-(-\gamma) \rightarrow X + e^-(E_i^{++}{}' - \alpha - \beta - \gamma)$

F. Multistage processes

1.   RN(A2 $\rightarrow$) + AD(B1)

2.   RI(A2 $\leftarrow$) + AN(C1)

3.   RN(A3 $\rightarrow$) + AI(D) + AN(C1)

the ground-state neutral particle, process $(1a\leftarrow)$
in Table I is the only electronic transition process
possible to an atomic particle which is not carrying
potential energy. It underlies the important field
of surface ionization mentioned above.

Categories B, C, and D of Table I illustrate
Auger-type processes in which two electrons under-
go transitions from one energy level to another.
These are Auger deexcitation (AD), Auger neu-
tralization (AN), and autoionization (AI), which is
also an Auger-type process. In AD processes
(category B) one of these electrons originates in the
solid and the other in the atom. In AN processes
(category C) both electrons originate in the solid,
and in the AI processes (category D) both originate
in the atom. Thus these three categories repre-
sent all types of Auger process possible if the en-
ergy E_k of the excited electron, written generally
$e^-(E_k)$, places it either in unfilled levels below the
vacuum level $-\phi < E_k < 0$ for a metal, or in the con-
tinuum above the vacuum level $E_k > 0$. An electron
will be ejected only if $E_k > 0$ and then only if it is
directed so as to have sufficient momentum normal
to the solid surface to surmount the energy barrier
there.

In category E of Table I we have listed a possible
ion-neutralization process for doubly charged ions
involving three electrons. Also, in category F we
list three multistage processes of interest in the
present work using a notation which refers to the
categories specified earlier in the table.

The present work deals with processes possible
for the incident particles $He^+(2s)$ and He^{++}. The AI
process, category D of Table I, has been observed
and identified for the first time in this work in the
multistage process F3. We shall discuss the iden-
tification and energetics of the processes observed
as well as the kinetics of processes which compete
with each other as the incident atomic particle ap-
proaches the solid surface.

III. EXPERIMENTAL APPARATUS AND PROCEDURES

The apparatus used in the present work is that
currently being used in our work on the electronic
characterization of solid surfaces by ion-neutrali-
zation spectroscopy.[27] In it a focused, essentially
monoenergetic, slow-ion beam ejects electrons
from a single-crystal target, T in Fig. 1, having
a well-characterized surface. These ejected elec-
trons are analyzed as to their kinetic energy by re-
tarding potentials placed between a spherical grid
S_1 and a spherical collector S_2 also shown in Fig.
1. We include Fig. 1 for use in discussing the de-
tails of our operation of this analyzer. Our first
use of this analyzer was mentioned briefly in Ref.
25.

First let us discuss the ion beam which enters
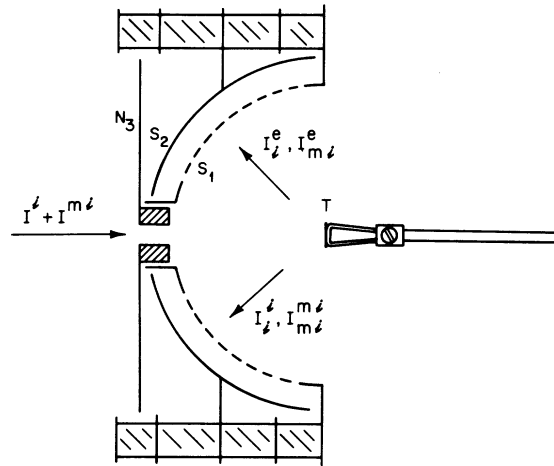the target-collector system of Fig. 1 from the ion

FIG. 1. Schematic diagram of the experimental arrange-
ment of target T and spherical electron energy analyzer
consisting of grid S_1 and collector S_2. Principal space
currents are designated using a notation in which the
character of the particle current (e, electron; i, ion; mi,
metastable ion) is indicated by the superscript and the
particle to which the current is secondary is indicated by
the subscript.

source and ion lens portions of the apparatus (see
Fig. 6 of Ref. 27). It is formed from the parent
He gas by electron impact in a crossed electron
beam. It can consist of pure $He^+(1s)$, mixed $He^+(1s)$
$+ He^+(2s)$, or He^{++} with a relatively small admixture
of the He^+ ions. Pure $He^+(1s)$ is obtained when the
electron beam is operated below the onset potential
(65.4 eV) for production of $He^+(2s)$ in a single elec-
tron collision. The combined beam with the largest
proportion of $He^+(2s)$ is obtained with the electron
beam energy at 120 eV which we have determined
as being near the maximum of the $He^+(2s)$ ioniza-
tion efficiency curve. We further increased the
relative amount of $He^+(2s)$ by reducing all ion ac-
celerating or decelerating fields used in the ion
lenses of the apparatus to the smallest values con-
sistent with their proper operation. We were able
to reduce electric field quenching of the metastable
ion severalfold in this way. Although we cannot
separate $He^+(2s)$ from the $He^+(1s)$ we can separate
their ejected electron progeny by energy analysis
as discussed below. The mixed ion beam consisted
of 99.9% $He^+(1s)$ and 0.1% $He^+(2s)$. He^{++} was sep-
arated from the largest portion of the He^+ beam in
the electron-beam-collimating magnetic field by
virtue of the difference in mass to charge ratio.
Although not all He^+ was eliminated from the He^{++}
beam in this way, the relative amount of $He^+(2s)$
which produces ejected electrons in the same en-
ergy range as those ejected by He^{++} was negligible.

The principal space currents which flow in the
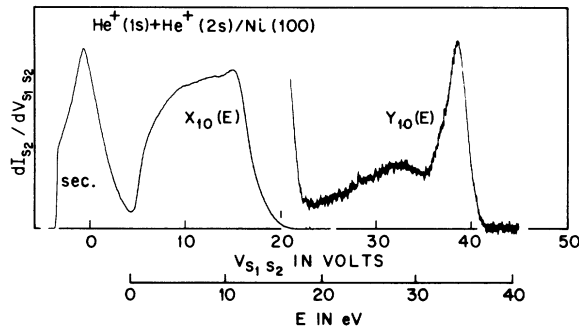target-collector region of the apparatus are de-

FIG. 2. Photographically reproduced plot of $dI_{S_2}/dV_{S_1S_2}$ for a 10-eV beam of mixed $He^+(1s)$ and $He^+(2s)$ ions incident on an atomically clean Ni(100) surface. The peak near $V_{S_1S_2}=0$ labeled "sec." is due to secondary electrons ejected from the grid S_1. The $X_{10}(E)$ and $Y_{10}(E)$ curves are, respectively, the kinetic energy distributions of the electrons ejected by $He^+(1s)$ and $He^+(2s)$ ions at the target surface as explained in the text. The extrapolated low-energy onset of the $X_{10}(E)$ distribution is taken to define the zero of the E scale or the vacuum-level energy of the Ni(100) surface. The detection sensitivity for $Y_{10}(E)$ is 300-fold larger than that for $X_{10}(E)$.

picted in Fig. 1 for an incident ion beam consisting of the ground-state ion (current I^i) and the metastably excited ion (current I^{mi}). Currents leaving the target, which are inside and approaching electrode S_1, are the electron currents I_i^e and I_{mi}^e secondary to I^i and I^{mi}, respectively. In addition, some ground-state and excited ions are reflected at the target surface making up the currents I_i^i and I_{mi}^{mi}, respectively. Since all four of these currents can eject secondary electrons from the grid S_1 it is necessary to take steps to separate these grid secondaries from the electron currents I_i^e and I_{mi}^e which we wish to analyze. This is done by accelerating ions approaching T and electrons receding
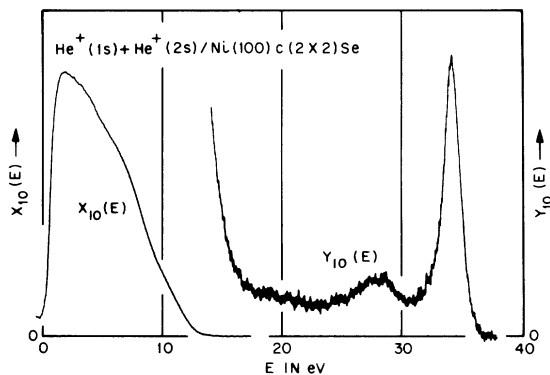

FIG. 3. Photographically reproduced $X_{10}(E)$ and $Y_{10}(E)$ distributions for a 10-eV beam of He^+ (1s) and He^+ (2s) incident on the Ni(100)c(2 × 2)Se surface.
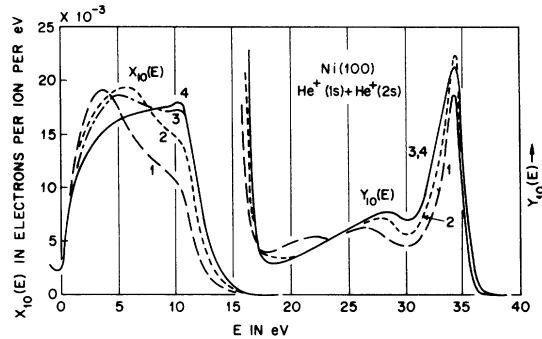

FIG. 4. Traced X and Y distributions for 10-eV $He^+(1s)$ and $He^+(2s)$ on Ni(100) with various amounts of adsorbed background gas present upon it. Corresponding X and Y distributions are labeled with the same number. In the sequence of curves 1–4 the surface coverage decreases from a large fraction of a monolayer, curve 1, to a value of the order of 0.01 monolayer, curve 4, for the clean surface.

from T each by a potential of 5 V applied between the common N_3, S_1 electrodes, and T. This seperates the electrons ejected from T and S_1, as can be seen in Fig. 2.

Three components of the electron current reaching S_2 are clearly to be seen in Fig. 2. These are the secondaries formed at S_1, the $X_{10}(E)$ distribution due to $He^+(1s)$, and the $Y_{10}(E)$ distribution due to $He^+(2s)$. We note that $He^+(1s)$ is both present in the original beam and formed as an eventual deexcitation product of $He^+(2s)$. Although we cannot separate $He^+(2s)$ from $He^+(1s)$, we see that there is a window about 20-eV wide above the X distribution in which electrons of the Y distribution resulting solely from processes initiated by $He^+(2s)$ may be observed. We term the distribution of electrons in this window ejected by He^{++} the $Z(E)$ distribution.

The present experiment was performed applying the same standards of vacuum technique and surface preparation as have been applied in our work with ion-neutralization spectroscopy.[24,25] In Fig. 3 we show the X_{10} and Y_{10} distributions for $He^+(1s)$ + $He^+(2s)$ on the Ni(100) face with a c(2×2) structure of adsorbed Se atoms upon it. Here the $X_{10}(E)$ distribution is recognized as that for this surface analyzed in Ref. 24. Similarly, Fig. 4 shows X and Y distributions for the Ni(100) surface in various states of cleanness with respect to adsorbed atoms from background gases. Clearly both $X(E)$ and $Y(E)$ are sensitive to the specific state of the metal surface.

Electron currents to electrode S_2 as a function of $V_{S_1S_2}$ were detected by a Cary vibrating-reed electrometer whose output was differentiated using an operational amplifier to produce the $X(E)$, $Y(E)$, and $Z(E)$ distribution functions. Photographic reproductions of the x-y recorder plots of these func-
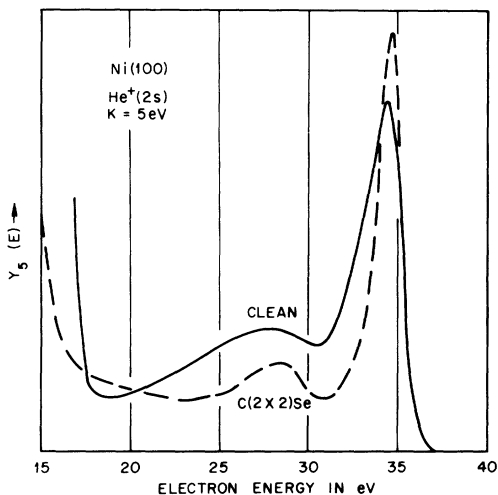
FIG. 5. Kinetic energy distributions of electrons ejected from the clean Ni(100) and the Ni(100)c(2 × 2)Se surfaces by 5-eV He$^+$(2s) ions.

FIG. 7. $X(E)$ and $Y(E)$ distributions for He$^+$(2s) incident on a Ni(100) surface covered with gas adsorbed from the background gases in the apparatus. The $Y(E)$ distribution is shown for several ion kinetic energies K.

tions are to be found in Figs. 2, 3, and 18. Curves in other figures are tracings of such data. We have also employed a multichannel scaler to average several runs of $Y(E)$ and $Z(E)$ distributions. An x-y recorder plot of such an average from the memory of the scaler is shown in Fig. 20 for electrons ejected by He^{++}.
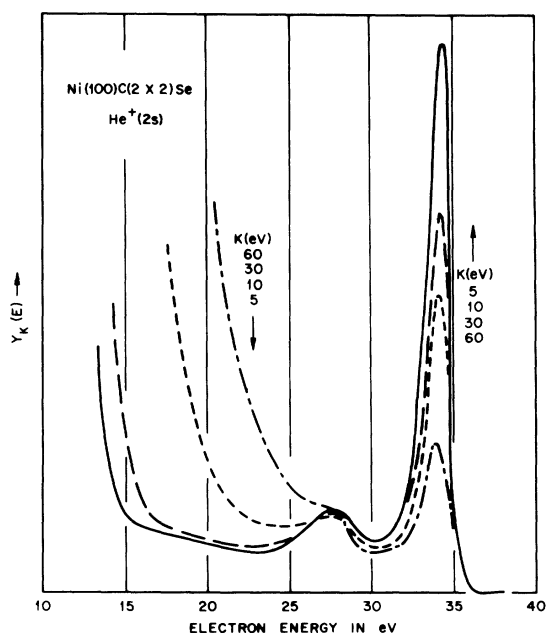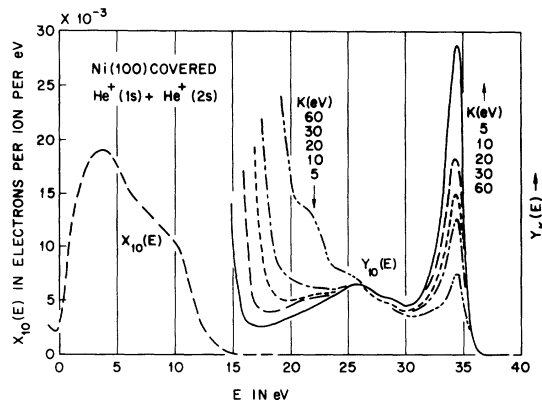
IV. EXPERIMENTAL RESULTS FOR INCIDENT He$^+$ (2s) IONS

The basic results of this work are the $Y(E)$ distributions determined for He$^+$(2s) incident ions of various kinetic energies K on various nickel surfaces. These data are to be found in Figs. 2–7. The $Y(E)$ distribution for clean Ni(100) shows a single large peak at an energy $E = 34.4$ eV above the vacuum level (Figs. 2 and 5). Coverage of the Ni(100) surface with background gas (Fig. 4) or with the c(2×2)Se structure (Fig. 5) narrows this peak and shifts it slightly to higher energy, $E = 34.6$ eV. Variation of K, the incident kinetic energy of the ions, is seen in Figs. 6 and 7 to reduce the peak height monatomically without changing its width or position.

Results for the Ni(110) surface, clean and with the c(2×2)Se superstructure, are seen in Figs. 8 and 9. With the surface clean (Fig. 8), $Y(E)$ shows a peak at $E = 34.2$ eV and a second smaller peak at

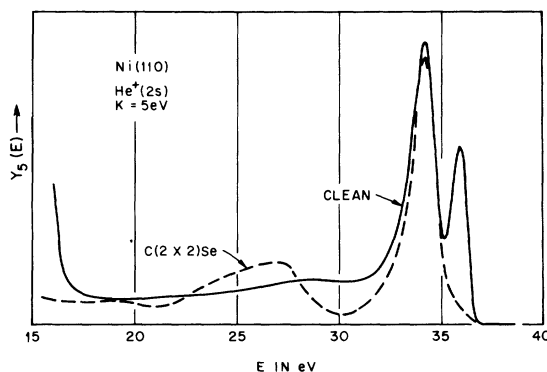FIG. 6. Variation of the $Y(E)$ distribution for the Ni(100)c(2 × 2)Se surface with kinetic energy K of the incident He$^+$(2s) ions.

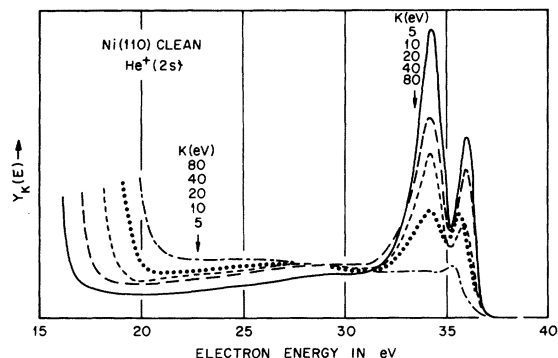FIG. 8. $Y(E)$ distributions for 5-eV He$^+$(2s) ions incident on the clean Ni(110) and the Ni(110)c(2 × 2)Se surfaces.

FIG. 9. Variation of the $Y(E)$ distribution for the clean Ni(110) surface with kinetic energy of the incident $He^+(2s)$ ion.

$E = 36.0$ eV. Coverage with $c(2 \times 2)$Se completely eliminates this higher energy peak leaving the lower energy peak at $E = 34.3$ eV, essentially where it was for the clean surface but somewhat narrower. Variation of $Y(E)$ with K for the clean Ni(110) surface (Fig. 9) shows both peaks diminishing in intensity monotonically with increasing K without change in peak width. Whereas the lower energy peak maintains its position on the energy scale during this diminution in intensity, the higher energy peak shifts to lower energy with increasing K. This is particularly apparent for $K > 20$ eV. All $Y(E)$ distributions show a broad peak near $E = 28$ eV. Structural features of the $Y(E)$ distribution obtained for incident $He^+(2s)$ ions are summarized in Table II.

In the discussions to follow we shall need the energies of ground and excited states of He atoms and ions listed in Table III. Column 1 of this table indicates the literature sources of the energies listed in columns 2 and 3 for the He states specified in column 4. For the doubly excited states He^{0**} the primary energy data are given in column 3. Columns 5–7 give energy intervals below the thresholds of three ionization continua. Other energies of interest are the work functions of the metal surfaces used in this experiment. The values we shall use are those from Ref. 25, listed in Table IV.

TABLE II. Structural features of $Y(E)$ for $He^+(2s)$.

| | | Energy in eV | | | |
| | | Ni(100) | | Ni(110) | |
States	Clean	$c(2 \times 2)$Se	Clean	$c(2 \times 2)$Se
$(E_k)_{max}$	⋯	33.6	36.6	36.7	36.5
E'_{k1}	$^1D + {}^1P$	⋯	⋯	36.0	⋯
E'_{k2}	$^1S + {}^3P$	34.4	34.6	34.2	34.3
E'_{k3}	⋯	28	28	(29)	27

V. PROCESSES BY WHICH He^+ $(2s)$ IONS EJECT ELECTRONS FROM A METAL SURFACE

There are a number of possible single-stage processes by which the excited $He^+(2s)$ ion could eject electrons from a metal surface. These are processes B3, C2, C3, and E of Table I. A two-stage ejection process is also possible, namely, process F3 consisting of resonance neutralization of $He^+(2s)$ to a doubly excited He^{0**} atom which, in turn, autoionizes to $He^+(1s)$ with the release of a fast electron.

Consider first process B3. It was in an attempt to observe this process of Auger deexcitation of the $He^+(2s)$ ion that we initiated the present study. Although our first determination of $Y(E)$ for Ni(100) looked superficially like the $U(\zeta)$ function obtained from $X(E)$ distributions by ion-neutralization spectroscopy (INS), further observation and experimentation indicated beyond doubt that electrons ejected by $He^+(2s)$ cannot come principally from this pro-

TABLE III. Energy levels and intervals in eV for He^0, He^+, He^{++}.

1 (Ref.)	2	3	4	5	6	7
a	79.0		He^{++}			0
a	76.8		$He^+(5s)$			2.2
a	75.6		$He^+(4s)$			3.4
a	72.9	48.3	$He^+(3s)$			6.1
a	65.4	40.8	$He^+(2s)$		0	13.6
b	64.2	39.6	$He^0(2s, 4s)^1S$		1.2	
c, d, e	63.6	39.0	$He^0(23sp+)^1P$		1.8	
b	63.1	38.5	$He^0(2s_13p)^3P$		2.3	
b, d	62.9	38.3	$He^0(2s, 3s)^1S$		2.5	
c, e, f	60.1	35.5	$He^0(2s, 2p)^1P$		5.3	
c, d, g	60.0	35.4	$He^0(2p^2)^1D$		5.4	
h	59.7	35.1	$He^0(2p^2)^3P$		5.7	
b–e	58.3	33.7	$He^0(2s, 2p)^3P$		7.1	
b–e	57.9	33.3	$He^0(2s^2)^1S$		7.5	
a	24.6	0	$He^+(1s)$	0	40.8	54.4
a	22.9		$He^0(1s, 3s)^1S$	1.7		
a	22.7		$He^0(1s, 3s)^3S$	1.9		
a	20.6		$He^0(1s, 2s)^1S$	4.0		
a	19.8		$He^0(1s, 2s)^3S$	4.8		
a	0		$He^0(1s^2)^1S$	24.6	65.4	79.0

[a]C. E. Moore, *Atomic Energy Levels*, Nat. Bur. Std. Circular No. 467 (U.S. GPO, Washington D.C., 1949).

[b]M. E. Rudd, Phys. Rev. Lett. 15, 580 (1965).

[c]J. A. Simpson, S. R. Mielczarek, and J. Cooper, J. Opt. Soc. Am. 54, 269 (1964).

[d]N. Oda, F. Nishimura, and S. Tahira, Phys. Rev. Lett. 24, 42 (1970).

[e]J. A. Simpson, G. E. Chamberlain, and S. R. Mielczarek, Phys. Rev. 139, A1039 (1965).

[f]R. P. Madden and K. Codling, Astrophys. J. 141, 364 (1965).

[g]H. G. Berry, J. Desesquelles, and M. Dufay, Phys. Rev. A 6, 600 (1972).

[h]J. L. Tech and J. F. Ward, Phys. Rev. Lett. 27, 367 (1971).

cess. We now summarize our reasons for this con-
clusion.

The peak at $E = 34.4$ eV in the $Y_5(E)$ distribution
for clean Ni(100), shown in Fig. 5, has a width at
half-maximum of about 3 eV, which is at least 50%
greater than the d bandwidth to be seen in Fig. 12
of Ref. 28. Second, we observe in Fig. 5 that ad-
sorption of the $c(2\times)$Se structure does not dimin-
ish the intensity of the peak as it does the d band in
the $U(\zeta)$ distribution obtained for this surface by
INS (see Fig. 12 of Ref. 24 and Fig. 10 here.)
Third, Figs. 6 and 7 indicate that the peak in the
$Y(E)$ distribution drops rapidly in intensity with ion
kinetic energy K. This is definitely not what we
would expect to occur if this peak consisted of d-
band electrons ejected in process B3 of Table I.
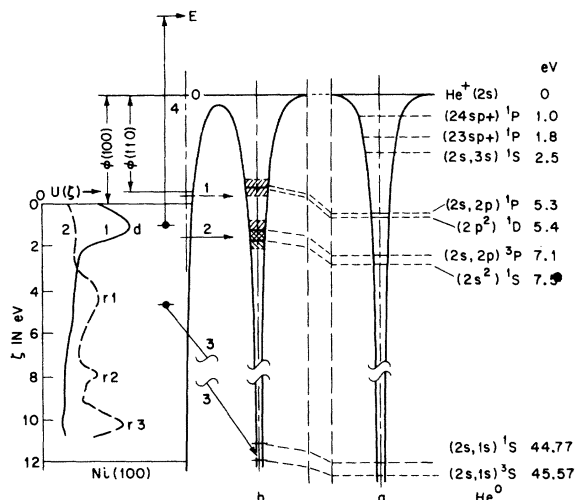Increased kinetic energy of the incident ion would

FIG. 10. Electron energy diagram showing states of
the doubly excited He^{0**} atom appropriate to resonance
tunneling for incident He$^+(2s)$. Energies below the He$^+(2s)$
ionization limit at the vacuum level are given for the
particle in free space (position a) to the right-hand side of
of the electron configurations. Energy levels shift up
when the particle comes near to the surface as shown at
position b. Two groups of such states ($^1S + ^3P$) and
($^1D + ^1P$) are possiblities for resonance tunneling from
He$^+(2s)$. Resonance transitions into these states via pro-
cess A3 of Table I are shown by arrows 1 and 2. Arrows
3 and 4 show the down and up transitions appropriate to
the AN process C2 of Table I. Fermi-level positions
appropriate to the atomically clean Ni(110) and Ni(100)
surfaces are shown and work functions for these surfaces
are indicated. In the panel to the left, $U(\zeta)$ functions for
the clean Ni(100) surface (curve 1) and for the Ni (100)
$c(2\times 2)$Se surface (curve 2) are shown. These are from
the work of Ref. 24. The d-band peak in curve 1 is in-
dicated by the letter d. r1, r2, and r3 in curve 2 indicate
three resonances due to electrons in surface orbitals of
the Se atom bound to the Ni surface. Compare these
curves of $U(\zeta)$ for Ni(100) with those for Ni(110) in Fig.
21.

TABLE IV. Surface work functions.

Surface	Work function (eV)
Ni(100)	5.1
Ni(100) $c(2\times 2)$Se	5.4
Ni(110)	4.7
Ni(110) $c(2\times 2)$Se	5.1

cause this process to occur closer to the solid sur-
face where in that case we would expect the d-band
wave functions to increase in magnitude relative to
the s and p wave functions of the conduction band of
nickel. Finally, we see in Figs. 8 and 9 that the
$Y(E)$ distribution for He$^+(2s)$ incident on atomically
clean Ni(110) has two peaks near its energy maxi-
mum rather than one. Such a result clearly can-
not result from process B3 given the local density
of surface electrons determined for Ni in Ref. 28.

Processes C2 and C3 are both two-electron Auger
processes, each of which requires that the mea-
sured $Y(E)$ distribution be related to the self-con-
volution of the local density of states of the metal
surface. It is clear from the work of Ref. 28 that
this cannot be the case for distributions of the form
of those in Figs. 5-9. In addition to this, process
C3 would produce electrons of maximum energy
considerably larger than that observed. The same
objections raised to process C3 apply also to pro-
cess E of Table I. Processes A3 and C2, although
they cannot account for the large peak or peaks in
the observed electron distributions could, as we
shall see, play roles as secondary processes com-
peting with the dominant process.

We are left with a multistage process as the only
remaining possibility for accounting for our exper-
imental results. This is process F3 of Table I,
which consists of the resonance neutralization (RN)
process A3 → followed by the autoionization (AI) pro-
cess D. On this interpretation, the sharp peaks
observed in the $Y(E)$ distributions are made up of
electrons ejected from the He^{0**} atoms when they
autoionize near the metal surface after having been
formed by resonance tunneling of a metal electron.
Table III indicates that more than one such doubly
excited state is available in the appropriate energy
range. Whether one sees one or two or more peaks
must be determined by the energetic availability of
the He^{0**} states to the tunneling process as dis-
cussed in the Sec. VI.

VI. ENERGETICS OF TWO-STAGE ELECTRON-EJECTION PROCESS

There are several questions which can be posed
concerning the energetics of the resonance tunnel-
ing and autoionization processes. The present
work provides answers which illuminate in more
detail than has been possible previously the details

TABLE V. Autoionization lifetimes of isolated He^{0**} atoms.

State	Lifetime in (sec)
$He^0(2s^2)^1S$	4.7×10^{-15} [a], 7.0×10^{-14} [b]
$He^0(2s,2p)^3P$	6.2×10^{-14} [a]
$He^0(2p^2)^3P$	$\sim 10^{-6}$ [c]
$He^0(2p^2)^1D$	not available
$He^0(2s,2p)^1P$	1.5×10^{-14} [a]

[a]Theory of P. G. Burke and D. D. McVicar, Proc. Phys. Soc. Lond. 86, 989 (1965).
[b]Experiment of H. G. Berry, J. Desesquelles, and M. Dufay, Phys. Rev. A 6, 600 (1972).
[c]Theoretical estimate by E. Holöien, Ref. 29.

of atom-solid electronic interactions. A first such question relates to what states of He^{0**} are available for resonance tunneling. In Table III we have listed the nine lowest-lying doubly excited He^{0**} states. Eight of these nine states are so-called "weakly quantized states"[29] having lifetimes with respect to autoionization in the range $10^{-14} - 10^{-15}$ sec for the free atom (Table V). The ninth, $He^0(2p^2)^3P$, is a so-called "exactly quantized state" whose lifetime can exceed even that of a radiating state by orders of magnitude[29] (see Table V).

Taking into account the fact that we expect the He^{0**} levels to rise relative to the vacuum level as the particle approaches the solid surface, we have indicated in the electron energy diagram of Fig. 10 which He^{0**} states should be involved. (See Ref. 30 for a discussion of the variation of atomic levels near a surface.) All four of the energy levels shown will become broadened resonances of the combined metal-atom system as the wave functions of the two components of this system overlap. The characteristic broadening of these resonances will undoubtedly cause each of the pairs of levels $[(2s^2)^1S$ and $(2s,2p)^3P$, separated by 0.4 eV in the free atom, and $(2p^2)^1D$ and $(2s,2p)^1P$, separated by 0.1 eV in the free atom] to coalesce into single resonances near the surface. The tunneling transitions into these combined levels are indicated by arrows 1 and 2 in Fig. 10. The experimental results require that when $\phi \geq 5.1$ eV, as it is for the Ni(100), Ni(100)$c(2\times2)$Se, and Ni(110)$c(2\times2)$Se surfaces, only the combined state $(^1S + {}^3P)$ lies below the Fermi level and can be filled by resonance tunneling. When $\phi = 4.7$ eV, as it is for Ni(110), it must be true that at least the lower portion of the resonance formed from the $(^1D + {}^1P)$ states lies below the Fermi level and can also be filled by tunneling. Note that the separation between the two peaks for clean Ni(110) (peaks 1 and 2 in Table II) is observed to be 1.8 eV, only slightly smaller than the free space separation between the average positions of the

pairs of states $(^1S + {}^3P)$ and $(^1D + {}^1P)$.

We have concluded that the two two-stage processes we observe are

$$He^+(2s) + e_S^- \rightarrow He^0(^1D, {}^1P) \rightarrow He^+(1s) + e^-(E_{k1}), \quad (1)$$

$$He^+(2s) + e_S^- \rightarrow He^0(^1S, {}^3P) \rightarrow He^+(1s) + e^-(E_{k2}). \quad (2)$$

Autoionization processes for the free atom have been observed by others for all four of the He^{0**} states involved in Eqs. (1) and (2) and the kinetic energies of the ejected electrons measured. These yield the experimental values for the excitation energies listed in column 3 and referenced in column 1 of Table III, which are also the kinetic energies of electrons ejected on autoionization of the free atom. Taking E_{k1} and E_{k2} each as the averages of the free-space values for the two processes involved, we obtain $E_{k1} = 35.45$ eV and $E_{k2} = 33.5$ eV. In our experiment we see electrons from both processes (1) and (2) above only for the clean Ni(110) surface. Here we have found $E'_{k1} = 36.0$ eV and $E'_{k2} = 34.2$ eV. Thus the experiment yields the interesting result that electrons originating in an atomic autoionization process occurring when the atom is close to a metal surface on an atomic scale are faster than those ejected in the same processes in free space.

A detailed discussion of the energetics of both resonance tunneling and autoionization processes may be carried out with the help of the potential energy diagram of Fig. 11. At the right in this figure are plotted the energy levels of the total system appropriate to infinite atom-solid separation ($s = \infty$) for the initial, intermediate, and final states of the two-stage RN+AI process. Each of these levels will vary with s depending on the nature of the atom-solid interaction. For the atomic states this interaction is principally the image force between ion and solid. The He^{0**} interacts with the solid principally via a van der Waals force.

Curve 1 of Fig. 11 is for the initial state of the two-stage process in which the electron in the solid is taken to be at the vacuum level. Curves 2–5 are for the initial state with the electron in the solid at that level $-\alpha$ below the vacuum level which causes each curve to intersect its corresponding He^{0**} curve, curves 6–9, respectively, at the distance s_{tr} from the solid surface. These intersections of $He^+(2s)$ and He^{0**} interaction curves are indicated by the open circles. Since no electron is ejected in the resonance neutralization of $He^+(2s)$ the Franck-Condon principle requires that the process occur at a crossing of the initial- and final-state potential curves which we have taken to occur at s_{tr} in each case. Autoionization will occur closer to the metal, at s_{ta} let us say, where a transition is made from one of curves 6–9 to the final-state curve 10. The vertical energy separation between

one of curves 6–9 and curve 10 at $s = s_{ta}$, again by virtue of the Franck-Condon principle, is the kinetic energy E'_k of the autoionized electron.

The two-stage RN + AI process is particularly interesting energetically because of the consistency required between the energetics of the two component processes. Let us for the moment take the expressions for image and van der Waals interactions used in our previous publications, returning later to a discussion of their appropriateness as indicated by more recent work. Thus we take $-3.6/s$ as the image interaction in eV with s in Å. For the van der Waals interaction we use Prosen and Sachs's formula[31] $(-2\pi)^{-3}\alpha e^2 \pi k_m s^{-2}\ln(2k_m s)$ with k_m calculated as $(2m\epsilon_F)^{1/2}/\hbar$ using $\epsilon_F = 10$ eV and with a value of $\alpha = 23.2\times10^{-25}$ cm^3 estimated for $He^0(2s^2)$
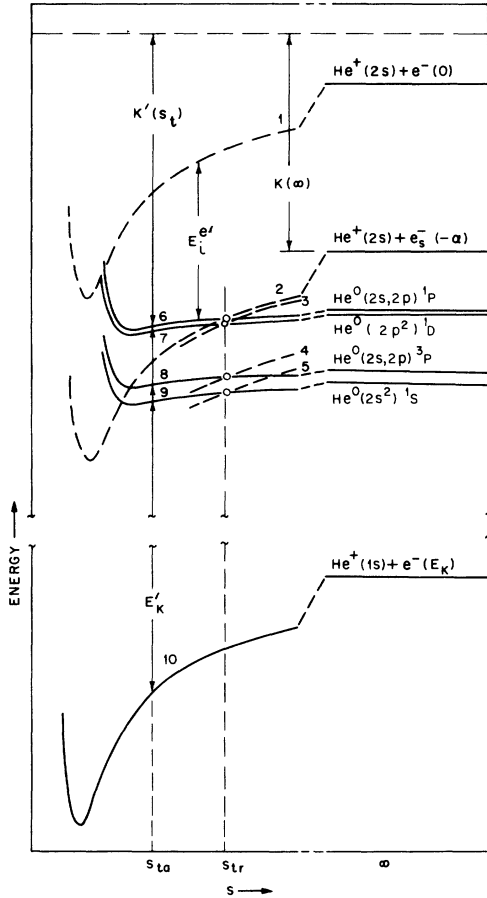

FIG. 11. Potential energy diagram illustrating the energy variation with atom-solid separation s of initial, intermediate, and final states in the processes of Eqs. (1) and (2). Relative positions of the states in free space ($s = \infty$) are indicated at the right-hand side where the isoelectronic atomic and electronic components are specified. How transitions among these curves proceed is discussed in the text. s_{tr} is the atom-solid separation at which the resonance transition occurs, s_{ta} that at which the Auger transition occurs.

from the value of $\alpha = 2.16\times10^{-25}$ cm^3 for $He^0(1s^2)$ on the basis that α varies inversely as the square of the ionization energy.[30] Using these expressions and the relationships indicated by Fig. 11 we may write the ionization energy of the He^{0**} state, $E_i^{e'}(s_{tr})$, at the atom-solid separation s_{tr} in terms of the free-space ionization energy of this state, $E_i^e(\infty)$, as

$$E_i^{e'}(s_{tr}) = E_i^e(\infty) - 3.6/s_{tr} + 0.64s_{tr}^2\ln(2.5s_{tr}) . \quad (3)$$

Similarly, Fig. 11 enables us to write the kinetic energy of the autoionized electron, $E'_k(S_{ta})$, produced in the AI process at $s = s_{ta}$, in terms of the kinetic energy $E_k(\infty)$, which these electrons would have if the process occurred at $s = \infty$, as

$$E'_k(s_{ta}) = E_k(\infty) + 3.6/s_{ta} - 0.64s_{ta}^2\ln(2.5s_{ta}) . \quad (4)$$

From expressions (3) and (4) we conclude the following: (i) The kinetic energy of the autoionized electrons is greater when the process occurs near a solid surface than in free space, and (ii) the upward shifts of the levels of the doubly excited states are equal to the increase in the ejected electron's kinetic energy over the free-space value if $s_{ta} \simeq s_{tr}$. These qualitative conclusions are clearly in agreement with our experimental results. Using the peak positions observed for Ni(110) we find the kinetic energy increase to be $34.2 - 33.5 = 0.7$ eV $= E'_k - E_k$, with the image term $+0.77$ eV and van der Waals term 0.07 eV. Putting this number into Eq. (4) we find $s_{ta} \cong 4.7$ Å. Had we used, as in Ref. 26, the average of the peak positions for E'_{k_2} in Table II, namely, 34.4 eV, we would have found $E'_k - E_k = 0.9$ eV and $s_{ta} \cong 3.6$ Å, with the image term $+1.1$ eV and the van der Waals term 0.11 eV. In either case we can conclude that the autoionization process occurs farther from the surface than does Auger neutralization of a ground-state ion (process C1 in Table I).[30]

The specific energies for use in Eq. (3) depend upon the distance s_{tr} at which the resonance tunneling occurs. Taking $s_{tr} \simeq s_{ta}$, which means that autoionization occurs very soon after tunneling, we find that the He^{0**} excited levels should shift up by an amount $E_i^e - E_i^{e'} = E'_k - E_k$ which we shall take to be 0.7 eV in the subsequent discussion. A shift of this magnitude leaves the $(^1S + ^3P)$ level well below the Fermi level for all surfaces used in this experiment. However, $E_i^e - E_i^{e'} = 0.7$ eV places the $(^1D + ^1P)$ level directly at the Fermi level for $\phi = 4.7$ eV [Ni(110)] but 0.4 eV above the Fermi level for $\phi = 5.1$ eV. These numbers come very close to satisfying the energetic requirements listed earlier for the RN process. They lead us to conclude not only that the picture of the RN + AI process afforded by Fig. 11 is essentially correct but that the numerical values used are also approximately correct. In addition, we realize that this picture re-

quires a rather fast autoionization process in order to make $s_{tr} \sim s_{ta}$, a point we return to in Sec. VII. In the preliminary publication[26] of this work we carried through this discussion on the basis of $E_k' - E_k = 0.9$ eV to which the reader is referred. The general conclusions reached are much the same. The $(^1D + ^1P)$ level now falls 0.2 eV above the Fermi level. This is perhaps an upper limit for its position at the moment of resonance tunneling if any appreciable fraction of the broadened resonance is to lie below the Fermi level.

We consider now the appropriateness of the specific formulations of image and van der Waals interactions used in Eqs. (3) and (4). Appelbaum and Hamann[32] have recently determined the image potential energy, in a one-parameter variational calculation, to be, in our notation, $-e^2/4(s - d)$. This is valid for s, the distance from the topmost plane of nuclei in the solid, greater than 2 Å. d has magnitude 0.26 Å. Thus our use of the simple $-e^2/4s$ form involves only a small shift of the two terms in Eqs. (3) and (4) relative to one another.

We realize that a number of formulations of the van der Waals term are to be found in the literature of which that by Prosen and Sachs is only one. Mavroyannis[33] has reviewed these formulas, presented two of his own, and tabulated the energies of interaction of rare-gas atoms and metal surfaces predicted by six different formulas. Five of these six formulas are in remarkable agreement, predicting the interaction energy of the Pt-He system at 2.70-Å separation to lie in the range 230–350 cal/mole, the mean of which is 0.013 eV. Taking, as before, the polarizabilities of He^{0**} and He^0 to be in the inverse ratio of their ionization energies, this number would correspond to 0.14 eV for the Pt-He^{0**} system in reasonable agreement with that used here. It is true that different formulas predict quite different variations with atom-solid separation, but we do not think our experiment can discriminate among these.

Finally, in this section we discuss the bearing of our results on the conclusions come to by MacLennan and Delchar (MD).[11] These authors conclude that the presence of an ion produced by resonance ionization of a metastable atom near a metal surface reduces the effective work function difference of the (111) and (110) faces of W to "almost zero" from the 1.6 eV measured in an ion-beam-retardation experiment. We point out that the present work requires that the $He^+(2s)$ ion incident on clean Ni(100) and Ni(110) does sence the 0.4-eV work-function difference of these surfaces. It is true that resonance neutralization of $He^+(2s)$ to $He^0(2s^2)$ probably occurs farther from the surface than does resonance ionization of $He^0(1s, 2s)$ to $He^+(1s)$ and would thus be less affected by the phenomenon MD describe. Two further points can be made. First,

it would appear that the ion in the ion-reflection experiment does detect the difference in the work function between the two W faces. This would appear to be inconsistent with the conclusion of MD that the ion-neutralization process cannot. Second, the energetics observed by MD for the electron ejection process are understandable if either the process occurring is predominantly Auger deexcitation of metastable atoms or photoemission. There are, to be sure, obvious difficulties with each of these interpretations.

VII. KINETICS OF THE TWO-STAGE ELECTRON-EJECTION PROCESS

There are several interesting points to be made concerning the kinetics of the two-stage process of electron ejection via resonance neutralization (RN) followed by autoionization. These concern the competition between the two-stage electron-ejection process and each of several other processes in which the potential energy of the incident particle is dissipated. We illustrate such competition among processes in Fig. 12. Here the two-stage process is indicated as a "reaction" proceeding horizontally from left to right across the top of the diagram. In competition with the RN process is an AN process in which $He^+(2s)$ is neutralized to the excited state $He^{0*}(1s, 2s)$ of the atom. In competition with the AI process is an AD process in which $He^{0**}(2s^2)$ is also converted to $He^{0*}(1s, 2s)$. As incident kinetic energy K is increased we expect the partition to shift toward greater probability of the AN and AD processes since all processes then occur closer to the surface.

The experimental results we intend to discuss are (i) the relative peak heights in the $Y(E)$ distribution of Fig. 9, (ii) the narrowing of the $(^1S + ^3P)$ resonance on adsorption of c $(2 \times 2)Se$, (iii) the monotonic decrease in peak height in all $Y(E)$ dis-
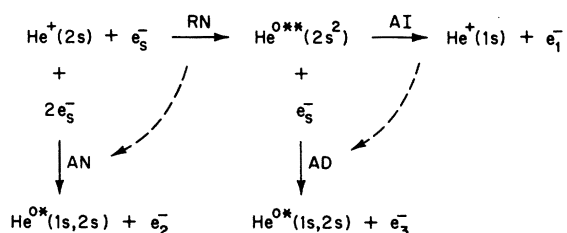

FIG. 12. The two-stage RN + AI process is indicated horizontally across the top of this figure with processes which compete with it at the initial and intermediate stages indicated vertically downward. The dashed circular arrows indicate the direction in which the partition is shifted as the kinetic energy (K) of the incident particle is increased. Subscripts 1, 2, and 3 have been added to the symbol e^- to distinguish the ejected electrons in the three processes shown.

tributions with increasing K, (iv) the insensitivity of peak widths to K, (v) the constancy in energy position of the lower energy peak (Figs. 6, 7, and 9), and (vi) the variation in position of the higher energy peak (Fig. 9) as K increases.

In the following discussions it will be instructive to consider two probability functions of the kind derived earlier on the basis that the transition probability per unit time has the form Ae^{-as}.[30] These are the probability $P_0^m(s, v_o)$ that an ion of incident velocity v_o will reach s without change of identity when process or processes m are possible, and the probability $P_{tn}^m(s, v_o)$ that process n will occur in the distance increment ds at s under the same conditions. Process n is either identical to process m if only one process can occur or is one of the several competing processes indicated by m. If we let $n = 1$, 2, 3 stand for the processes RN, AN, and RN + AI, respectively, P_0^1 is the P_0 probability of process 1 when process 1 only is allowed, P_{t2}^{2+3} is the P_t probability of process 2 when processes 2 *and* 3 are allowed to compete with each other, and so forth.

The probabilities P_0^1 and P_{t1}^1 are obtained from Ref. 30 as

$$P_0^1(s, v_0) = e^{-a_1(s - s_m^1)} \tag{5}$$

and

$$P_{t1}^1(s, v_0) = a_1 \exp\left[e^{-a_1(s - s_m^1)} - a_1(s - s_m^1)\right], \tag{6}$$

in which s_m^1 is the position of the maximum of the P_{t1}^1 function given by

$$s_m^1 = (1/a_1)\ln(A_1/a_1 v_0). \tag{7}$$

Expressions (5) and (6) also apply to process 2. P_0^3 and P_{t3}^3 for process 3 (RN + AI), on the other hand, are

$$P_0^3(s_1 v_0) = P_0^1(s_1 v_0) \tag{8}$$

and

$$P_{t3}^3(s, v_0) = \int_s^\infty P_{t1}^1(s_t, v_0) e^{-(s_t - s)/v_0 \tau} ds_t / v_0 \tau. \tag{9}$$

Equation (9) is derived from the condition that the AI process of lifetime τ occurs at s with probability $e^{-(s_t - s)/v_0 \tau}$ if the RN process which must precede it occurs at s_t.

Now let us allow processes 2 and 3 to compete. This, of course, involves competition of processes 1 and 2. Under these circumstances the following expressions may be derived:

$$P_0^{1+2} = P_0^{2+3} = P_0^1 \times P_0^2, \tag{10}$$

$$P_{t1}^{1+2} = P_{t1}^{2+3} = a_1 \exp\left[- e^{-a_1(s - s_m^1)} \right.$$
$$\left. - e^{-a_2(s - s_m^2)} - a_1(s - s_m^1)\right], \tag{11}$$

and

$$P_{t3}^{2+3} = \int_s^\infty P_{t1}^{2+3} e^{-(s_t - s)/v_0 \tau} ds_t / v_0 \tau. \tag{12}$$

We are now able to distinguish two extreme cases of Eq. (9) based on the relative widths of the $P_{t3}^3(s, v_0)$ function and the function $e^{-(s_t - s)v_0 \tau}$, $s_t \geq s, 0$, $s_t \leq s$. The full width of the P_t function at half-maximum is $2.48/a$ and the exponential falls to $1/e$ of its value in a distance $v_0 \tau$ which we take to be its "width."[30] Then if $2.48/a_1 \ll v_0 \tau$ the distance increment required for large probability that the AI process will occur is large relative to the width of the P_{t1}^1 function. In this limit we expect most of the doubly excited atoms to be deexcited by a collision with the lattice rather than by autoionization with the ejection of an electron. In the other extreme, $2.48/a_1 \gg v_0 \tau$, AI occurs very soon after RN and $P_{t3}^3 \simeq P_{t1}^1$.

We now return to a discussion of the experimental results listed earlier in this section. The smaller magnitude of the peak at $E = 36.0$ eV relative to that of the peak at $E = 34.2$ eV in Fig. 9 could result in part at least from the fact that the resonance due to the $(^1D + {}^1P)$ states of He^{0**} overlaps the Fermi level as illustrated in Fig. 13. A second reason could be that probability of resonance tunneling into $(^1D + {}^1P)$ is reduced by the possibility of resonance tunneling into a broadened resonance arising from the non-autoionizing level $He^0(2p^2){}^3P$ which lies only 0.3 eV below ^1D (Table III).

Next consider a possible reason why the $(^1S + {}^3P)$ resonance at $E \simeq 34.4$ eV narrows when the $c(2\times 2)Se$
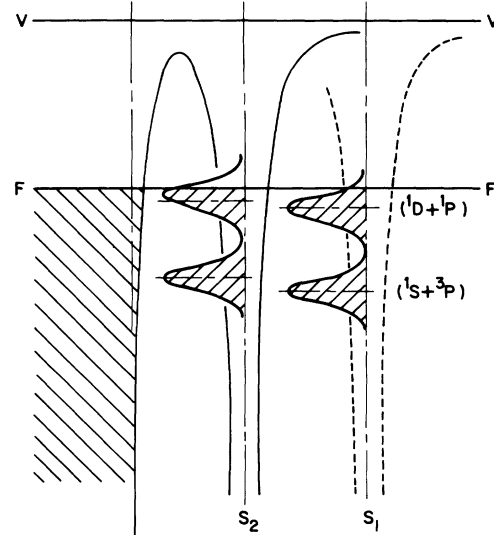

FIG. 13. Energy-level diagram showing the He^{0**} atom in two positions relative to the surface. The two resonances shown in each well are the resonances of electrons in the pairs of doubly excited states indicated. Note that as the atom moves from S_1 to S_2, part of the upper resonance rises above the Fermi level and that the center of gravity of its filled portion moves closer to the lower resonance.
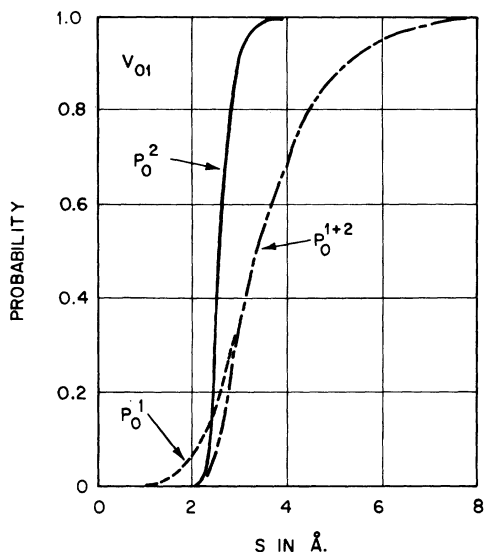
FIG. 14. Plots of P_0 functions for the lower velocity V_{01} of two used in an illustrative example of kinetic competition between two processes. Note that P_0^1 and P_0^2 overlap slightly. P_0^{1+2} is the over-all probability that the ion retain its initial identity to the distance s when processes 1 and 2 are operating and competing.

structure is formed on either the Ni(100) surface (Fig. 5) or the Ni(110) surface (Fig. 8). We believe this could be a result of the different local density of states at the surface of the solid with which the resonance formed of excited states in the incident atom interacts. We note in the left panel of Fig. 10 that the local density of states as given
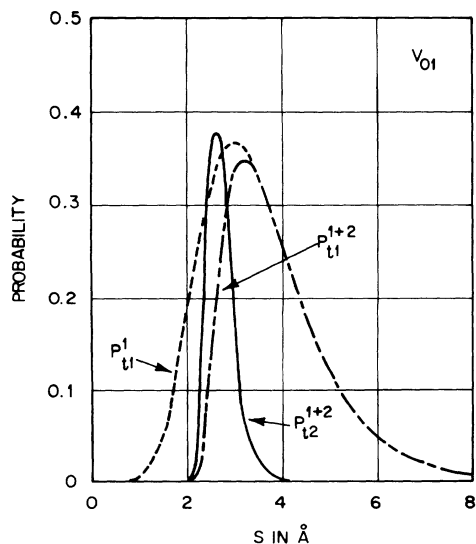
by the INS $U(\zeta)$ function has a relatively smaller d-band peak near $\zeta = 1$ eV when $c(2\times2)$ Se is present (curve 2) than when the surface is clean (curve 1, peak labeled d). This can only mean that the wave-function magnitude in the range of energies of the Ni d band is less at a given distance from the Se superstructure, when it is present, than it is at the same distance from the topmost Ni atoms when the surface is clean. This has two consequences. At comparable distances from the topmost atom layer (Se or Ni) the interaction of the filled $(^1S + {}^3P)$ state with the solid will be smaller with Se present resulting in a narrower resonance. This effect must be compensated for in part by the fact that the smaller wave-function magnitude requires closer approach before tunneling can occur. However, the kinetics appear to be such that narrowing of the resonance does occur when the $c(2\times2)$Se structure is formed.

The monotonic decrease in magnitude of all autoionization peaks with increasing K could result both from deexcitation by collision with the lattice and increasing competition from other processes as in Fig. 12 if the true situation lies somewhere between the extremes of relative rates of the RN and AI processes discussed above. We note that the autoionization peaks effectively disappear over an incident velocity $(\sqrt{K})$ variation of about 3. Because of its exponential variation, this large *ratio* of intensities can be approached in the limit of deexcitation by lattice collision only if essentially all doubly excited atoms are deexcited in this way at all velocities. We think the weight of evidence favors competing processes. A rough estimate of total yield gives about 0.3 electron from autoionization per incident $He^+(2s)$ ion. Furthermore the invariance with K of the width and position of the
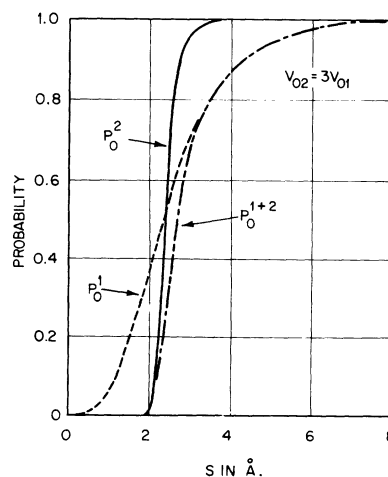

FIG. 15. P_t functions for the lower velocity case of Fig. 14.

FIG. 16. Plots of P_0 functions for the higher velocity $v_{02} \cong 3v_{01}$. Here P_0^1 and P_0^2 overlap considerably more than in Fig. 14.
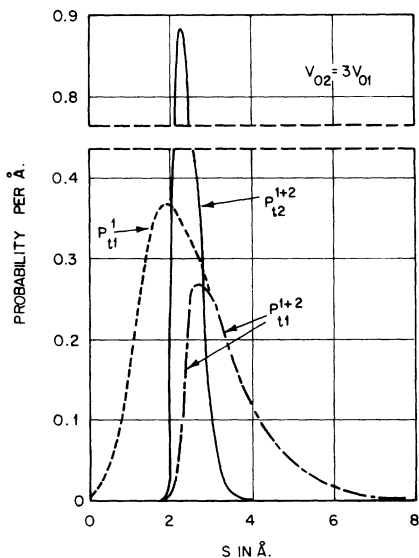
FIG. 17. P_t functions for the higher velocity case of Fig. 16.

FIG. 19. Variation of $Z(E)$ for He^{++} on $Ni(100)c(2 \times 2)Se$ with incident kinetic energy K of the He^{++} ion.

lower energy peak must mean that the energies in Eq. (4) are not varying greatly with K. This, in turn, would indicate a relatively high autoionization rate near the surface.

Competition between two processes, say, $1 = RN$ and $2 = AN$, requires overlapping P_0 and P_t functions. Thus the parameter a_1 in the rate $A_1 e^{-a_1 s}$ for process 1 must be smaller than the corresponding a_2 for process 2. This will assure that process 1 will occur over a narrower range of distances than process 2 and that its mean distance from the surface will vary more slowly with velocity. The A parameters, or the equivalent s_m parameter by Eq. (7), must be such as to cause process 2 to oc-
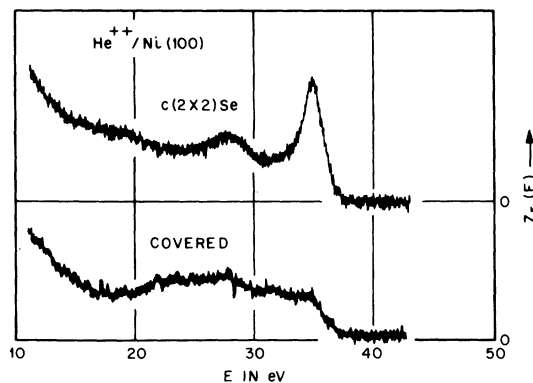
cur first as s decreases.

We have illustrated these kinetic requirements by means of an example based on the following parameters: $a_1 = 1$ Å^{-1}, $a_2 = 5$ Å^{-1}, $v_{01} = 2.2 \times 10^{14}$ Å/sec ($K = 10$ eV), $v_{02} = 3v_{01}$, $s_{m1}^1(v_1) = 3.0$ Å, $s_{m1}^2(v_1) = 2.5$ Å. Equation (7) becomes $s_{m1}^n - s_{m2}^n = (1/a_n)\ln(v_{02}/v_{01})$ for $n = 1$ and 2 from which $s_{m2}^1 = 2.0$ Å and $s_{m2}^2 = 2.3$ Å. Plots of P_0^1, P_0^2, and P_0^{1+2} for $v = v_{01}$ are given in Fig. 14. P_t functions for this case are shown in Fig. 15. We see that process 1 strongly predominates over process 2 as judged by the ratio of the areas of the P_{t1}^{1+2} and P_{t2}^{1+2} functions. When v is increased by a factor 3 to v_{02} the situation depicted in Figs. 16 and 17 prevails. Now process 2 is considerably more probable relative to process 1. In order to account for the large drop in autoionization peaks with increasing K it is probably necessary that more than one Auger process having the kinetic parameters like process 2 in this example be operative. This is suggested in Fig. 12.

A final point concerns the movement of the position of the higher energy peak in Fig. 9 toward lower energy as K increases. We believe this to be an effect also illustrated in Fig. 13. If the $(^1D + ^1P)$ resonance overlaps the Fermi level and rises as s_m decreases with increasing K the center of

FIG. 18. $Z(E)$ distributions for 5-eV He^{++} ions incident on $Ni(100)c(2 \times 2)Se$ (upper curve) and $Ni(100)$ covered with atoms from residual gases in the apparatus (lower curve).

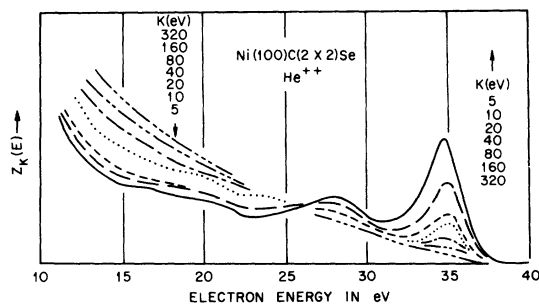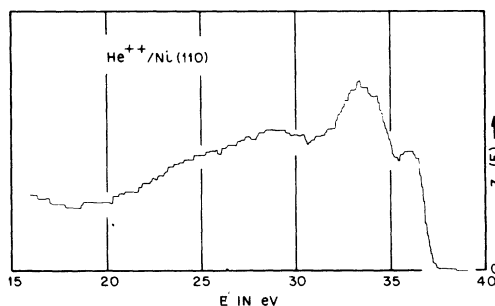FIG. 20. The $Z(E)$ distribution for He^{++} ($K = 5$ eV) incident upon clean $Ni(110)$. This curve is an X-Y recorder plot of points from several curves added and stored in the memory of a multichannel scaler.

TABLE VI. Structural features of $Z(E)$ for He^{++}.

		Ni(100)		Ni(110)	
	States	Clean	$c(2 \times 2)$Se	Clean	$c(2 \times 2)$Se
$(E_k)_{max}$	$\cdots$	37.1	37.4	37.0	37.0
E'_{k1}	$^1D + ^1P$	$\cdots$	$\cdots$	35.8	$\cdots$
E'_{k2}	$^1S + ^3P$	34.8	34.8	33.5	34.6
E'_{k3}	$\cdots$	(28)	28	(28)	27

gravity of that portion which is filled by resonance tunneling will, in fact, move closer to the lower ($^1S + ^3P$) resonance. This requires, of course, that the ^1D and ^3P levels have lost their atomic character and have in fact become overlapping resonances among the electronic states of the solid which are filled only to the Fermi level.

The general picture of the kinetics of competing processes which we have developed requires that autoionization occur at such a rate that $v_0\tau$ be of order 0.5 Å. For $v_0 = 2.2 \times 10^{14}$ Å/sec and the lifetime $\tau = 4.7 \times 10^{-15}$ sec listed for He$^0(2s^2)$ in Table V we obtain $v_0\tau \sim 1$ Å. Thus it appears that atomic autoionization must if anything be faster near a metal surface than it is in free space.

The processes indicated in Fig. 12 as competing with RN + AI are both two-electron processes. Thus the contribution of each to the $Y(E)$ distribution is in the form of the fold of the local density of states at the surface. This makes it difficult to predict the exact form of the distribution of electron energies and in particular to account for the maximum in $Y(E)$ near $E = 28$ eV.

VIII. RESULTS FOR INCIDENT He^{++} IONS

Experimental $Z(E)$ energy distributions for electrons ejected by He^{++} ions are presented in Figs. 18–20. Numerical data concerning structural features in these plots are given in Table VI. Comparison with Table II reveals a striking similarity in the energies at which these features appear. This is taken as a clear indication that the first process in which He^{++} participates as it approaches the Ni surface is resonance tunneling into the He$^+(2s)$ state. This would then be followed by all the competing processes discussed for He$^+(2s)$. Differences in intensity of the features in $Z(E)$ from those of $Y(E)$ might well be accounted for by the fact that He$^+(2s)$ and hence all its progeny are formed close to the surface because the He$^+(2s)$ state lies so low in the band in Fig. 21. As a result of this, all electron-ejection processes also occur closer to the surface than is the case for incident He$^+(2s)$.

In Fig. 21 we have plotted levels of the He$^+$ ion into which an electron from the solid might tunnel

to neutralize He^{++} by one electronic charge. We have also indicated approximate rises in these levels as the He$^+$ excited ion approaches the surface. Clearly the only contenders are He$^+(3s)$ and He$^+(2s)$. The first of these particles may be eliminated by considering the subsequent processes which would then occur and the energies which ejected electrons would then possess.

Resonance neutralization of He^{++} to He$^+(3s)$ might be followed by resonance neutralization to doubly excited levels in which one electron remains in the 3s state and the other electron occupies a level with principal quantum number $n = 2$. Several such states are listed in Table III. However, all such states lie below the He$^+(2s)$ ionization limit by considerably less than ϕ and hence are above the Fermi level and cannot be filled by tunneling from filled states.

Auger processes remain as possibilities. Those involving neutralization to He^{0**} states produce electrons no faster than 15.0 eV and those deexciting to He$^+(1s)$ or neutralizing to He^{0**} states produce electrons faster than 38.1 eV. Thus no conceivable neutralization or deexcitation process involving He$^+(3s)$ can account for the observed $Z(E)$
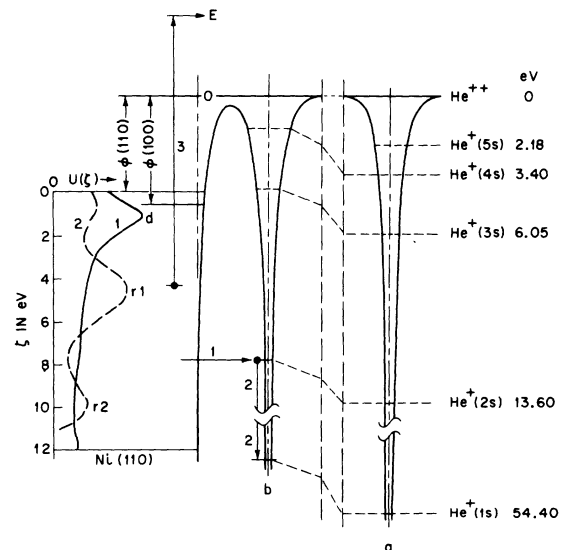

FIG. 21. Electron energy diagram illustrating the possible states of He^{++} into which electrons from Ni can tunnel as the He^{++} ion approaches the surface. States and energies below the He^{++} ionization limit are indicated at position a for $S = \infty$. Near the surface (position b) these states rise as is shown schematically. Arrow 1 indicates resonance tunneling into the He$^+(2s)$ state. Arrows 2 and 3 indicate the down and up electrons of process B3 of Table I for incident He$^+(2s)$. Work functions and $U(\zeta)$ functions from Ref. 25 for the clean (100) and (110) faces of Ni are indicated at the left in the figure.

distributions. Also, the three-electron process listed as process E in Table I would produce much faster electrons than are observed.

[1]M. Kaminsky, *Atomic and Ionic Impact Phenomena on Metal Surfaces, Struktur und Eigenschaften der Materie in Einzeldarstellungen* (Springer, Berlin, 1965), Vol. XXV, Chaps. 11–13.

[2]V. A. Abroyan, M. A. Eremeev, and N. N. Petrov, Usp. Fiz. Nauk **92**, 105 (1967) [Sov. Phys.-Usp. **10**, 332 (1967)].

[3]U. A. Arifov, *Interaction of Atomic Particles with a Solid Surface* (Nauka, Moscow, 1968) [English translation: Consultants Bureau (Plenum, New York, 1969)].

[4]*Secondary Emission and Structural Properties of Solids*, edited by U. A. Arifov (FAN, Tashkent, 1970) [English translation: Consultants Bureau (Plenum, New York, 1971)].

[5]D. W. Vance, (a) Phys. Rev. **164**, 372 (1967); (b) Phys. Rev. **169**, 252 (1968); (c) Phys. Rev. **169**, 263 (1968).

[6]M. Perdrix, J. C. Baboux, R. Goutte, and C. Guillaud, J. Phys. D **3**, 594 (1970).

[7]R. H. Prince and J. B. French, Rev. Sci. Instrum. **41**, 923 (1970).

[8]D. A. MacLennan, Phys. Rev. **148**, 218 (1966).

[9]R. N. Varney, Phys. Rev. **157**, 116 (1967).

[10]R. N. Varney, Phys. Rev. **175**, 98 (1968).

[11]D. A. MacLennan and T. A. Delchar, J. Chem. Phys. **50**, 1772 (1969).

[12]T. A. Delchar, D. A. MacLennan, and A. M. Landers, J. Chem. Phys. **50**, 1779 (1969).

[13]W. L. Borst, Rev. Sci. Instrum. **42**, 1543 (1971).

[14]F. B. Dunning, A. C. H. Smith, and R. F. Stebbings, J.

Phys. B **4**, 1683 (1971).

[15]F. B. Dunning and A. C. H. Smith, J. Phys. B **4**, 1696 (1971).

[16]W. Allison, F. B. Dunning, and A. C. H. Smith, J. Phys. B **5**, 1175 (1972).

[17]H. D. Hagstrum, Phys. Rev. **89**, 244 (1953).

[18]H. D. Hagstrum, Phys. Rev. **91**, 543 (1953).

[19]H. D. Hagstrum, Phys. Rev. **96**, 325 (1953).

[20]H. D. Hagstrum, Phys. Rev. **104**, 672 (1956).

[21]H. D. Hagstrum, Phys. Rev. **104**, 309 (1956).

[22]H. D. Hagstrum, J. Appl. Phys. **31**, 897 (1960).

[23]H. D. Hagstrum, Phys. Rev. **150**, 495 (1966).

[24]H. D. Hagstrum and G. E. Becker, J. Chem. Phys. **54**, 1015 (1971).

[25]G. E. Becker and H. D. Hagstrum, Surf. Sci. **30**, 505 (1972).

[26]H. D. Hagstrum and G. E. Becker, Phys. Rev. Lett. **26**, 1104 (1971).

[27]H. D. Hagstrum, Science **178**, 275 (1972).

[28]H. D. Hagstrum and G. E. Becker, Phys. Rev. **159**, 572 (1967).

[29]E. Holöien, Nucl. Instrum. Methods **90**, 229 (1970).

[30]H. D. Hagstrum, Phys. Rev. **96**, 336 (1954).

[31]E. J. R. Prosen and R. G. Sachs, Phys. Rev. **61**, 65 (1942).

[32]J. A. Appelbaum and D. R. Hamann, Phys. Rev. B **6**, 1122 (1972).

[33]C. Mavroyannis, Mol. Phys. **6**, 593 (1963).

Direct Measurement of an Order Parameter Associated with the 110.9-K Displacive Phase Transition in K₂ReCl₆†

Alan G. Brown and Robin L. Armstrong

Department of Physics, Toronto, Canada M5S-1A7

Kenneth R. Jeffrey

Department of Physics, University of Guelph, Guelph, Canada N1G-2W1

(Received 7 March 1973)

The temperature dependence of an order parameter associated with the 110.9-K displacive phase transition in K₂ReCl₆ is measured directly in the tetragonal phase using rotation patterns obtained from nuclear Zeeman quadrupole resonance studies on single crystals. The measurements extend over the temperature range $103 < T < 110.9$ K. The order parameter follows a Landau-like behavior to within 0.4 K of the transition temperature. The zero-temperature coherence length is calculated to be 9.2 Å, which is approximately the distance between adjacent ReCl₆ octahedra. Critical fluctuations in K₂ReCl₆ are therefore of short range.

I. INTRODUCTION

Several years ago O'Leary and Wheeler[1] published the results of a comprehensive study of the displacive phase transition occurring at 110.9 K in the antifluorite-type crystal K₂ReCl₆. X-ray diffraction, Raman scattering, infrared absorption, and pure nuclear quadrupole resonance measure-

ments all indicate that the phase transition involves a structural alteration which reduces the symmetry from cubic to tetragonal and that the phase transition is of the second order in the Landau sense.

Above 110.9 K each ReCl₆ octahedron occupies the center of a cubic cage defined by K ions. The principal axes of the octahedra are parallel to the